

# Applying Spectral Node Methodologies to Self-Intersecting Planar and Spherical Curves: An Extension of Erb's Rhodonea Framework

## Introduction

The mathematical characterization of sampling trajectories and their corresponding self-intersection points is a foundational problem in approximation theory, numerical analysis, and medical imaging. Classical spectral interpolation methods on bounded domains, such as the unit disk or the sphere, have traditionally relied on tensor-product grids in polar or spherical coordinates. However, modern scanning systems—such as those utilized in Magnetic Particle Imaging (MPI) or laser scanners employing rotating Risley prisms—rarely collect data on Cartesian or tensor-product grids. Instead, they often collect data continuously along complex, self-intersecting parametric curves.<sup>1</sup>

Wolfgang Erb's seminal work on rhodonea curves established a mathematically robust framework for utilizing these specific trajectories as sampling nodes for spectral interpolation.<sup>1</sup> By mapping the time-equidistant samples of rhodonea curves to a pair of interlacing polar grids, Erb demonstrated that the self-intersection and boundary points form a highly structured discrete orthogonality system. This system allows for unisolvant interpolation using a parity-modified Chebyshev-Fourier basis, effectively bypassing the limitations of tensor-product geometries.<sup>1</sup> Furthermore, this approach enables the implementation of fast Fourier algorithms, reducing the computational complexity of evaluating expansion coefficients to  $\mathcal{O}(m_1 m_2 \log(m_1 m_2))$ .<sup>1</sup>

The core analytical triumph of Erb's methodology is the reduction of transcendental phase collision problems—where a continuous trajectory crosses itself—into finite, solvable algebraic integer relations using mathematical tools such as Bézout's lemma.<sup>1</sup> This report investigates the theoretical and computational feasibility of extending Erb's node-finding algorithms and spectral interpolation techniques to a broader taxonomy of self-intersecting planar and spherical geometries. Specifically, the analysis evaluates the translation of this framework to Lissajous curves, epitrochoids, hypotrochoids, the generalized Gielis superformula with rational symmetries, and the Farris "mystery" curve.<sup>1</sup>

By systematically analyzing the algebraic varieties, parametric frequencies, trigonometric polynomial structures, and implicit equations underlying these shapes, this report synthesizes a generalized methodology for identifying self-intersection nodes. The ultimate objective is to

determine how these discrete sets of intersection points can be leveraged for high-order quadrature, rapid spectral convergence, and unisolvant interpolation across increasingly complex mathematical domains.

## The Foundations of Erb's Rhodonea Framework

To systematically evaluate the applicability of spectral node techniques to other curve families, it is first necessary to completely deconstruct the mathematical machinery Erb applied to rhodonea curves. Rhodonea curves, historically studied by Guido Grandi in the 18th century and frequently referred to as roses of Grandi, are classical planar curves confined to the unit disk  $\mathbb{D} = \{x \in \mathbb{R}^2 : |x| \leq 1\}$ .<sup>1</sup>

### Parametric Definition and Phase Collisions

Erb defines the rhodonea curve in parametric form as:

$$\rho_\alpha^{(m)}(t) = (\cos(m_2 t) \cos(m_1 t - \alpha\pi), \cos(m_2 t) \sin(m_1 t - \alpha\pi)) \text{ where}$$

$m = (m_1, m_2) \in \mathbb{N}^2$  represents the frequency vector and  $\alpha \in \mathbb{R}$  represents a rotation parameter.<sup>1</sup> These parameters dictate a superposition of a radial and an angular harmonic motion, making rhodonea curves polar variants of bivariate Lissajous curves.<sup>1</sup>

To extract all self-intersection points of the curve  $\rho_\alpha^{(m)}$ , one must consider the set of all temporal parameters  $t, s \in [0, 2\pi)$  such that the spatial coordinates align, meaning  $\rho_\alpha^{(m)}(s) = \rho_\alpha^{(m)}(t)$ .<sup>1</sup> Because the parametrization relies on the products of harmonic functions, any self-intersection necessitates a highly specific phase relationship between the arguments  $m_1 t$  and  $m_2 t$ . Setting the respective coordinates equal yields a system of trigonometric equalities. These equalities can only be satisfied if the arguments match up to integer multiples of  $\pi$  and parity shifts.

Specifically, Erb formulates these conditions as:  $m_2(s - ut) + \frac{1-v}{2}\pi \equiv 0 \pmod{2\pi}$   
 $m_1(s - t) + \frac{1-v}{2}\pi \equiv 0 \pmod{2\pi}$  for variables  $u, v \in \{-1, 1\}$ .<sup>1</sup>

The resolution of this continuous trigonometric system into a discrete grid relies on the application of Bézout's identity. Assuming the frequencies  $m_1$  and  $m_2$  are relatively prime, there exist integers  $a, b \in \mathbb{Z}$  such that  $am_1 + bm_2 = 1$ .<sup>1</sup> By multiplying the first phase equation by  $b$  and the second by  $a$ , and adding them together, the variables are

systematically decoupled. This algebraic manipulation yields exact, discrete time steps for sampling the curve:  $t_l^{(m)} = \frac{l\pi}{2m_1 m_2}$  where the index  $l$  iterates through the set  $\{0, 1, \dots, 4m_1 m_2 - 1\}$ .<sup>1</sup>

This sequence mathematically proves that all self-intersection points—as well as all points where the curve touches the exterior boundary of the unit disk—lie exactly on this time-equidistant grid.<sup>1</sup> For a relatively prime pair where  $m_1 + m_2$  is odd, the total number of node points (the union of self-intersections and boundary points) is exactly  $2m_1 m_2 + 1$ .<sup>1</sup> This includes the center of the disk  $(0, 0)$ , which acts as a highly degenerate singularity traversed  $2m_2$  times in one period, alongside  $2(m_1 - 1)m_2$  ordinary double points and  $2m_2$  boundary points.<sup>1</sup> If  $m_1 + m_2$  is even, the period halves to  $\pi$ , the center is traversed  $m_2$  times, and the curve contains  $\frac{1}{2}(m_1 - 1)m_2$  non-centric ordinary double points and  $m_2$  boundary points.<sup>1</sup>

## Algebraic Varieties and Discrete Orthogonality

Beyond the parametric time domain, Erb connects this formulation to an implicit algebraic variety representation. The rhodonea variety  $\mathcal{R}^{(m)}$  on the unit disk is defined as:

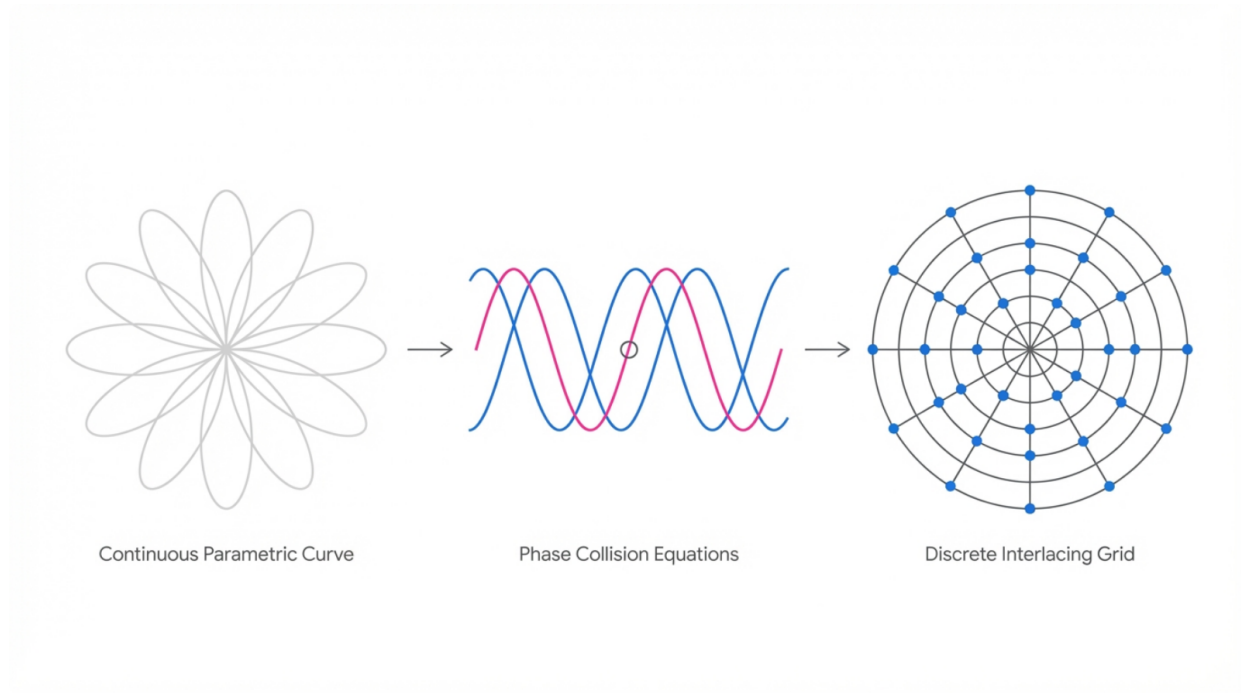
$$\mathcal{R}^{(m)} = \{x(r, \theta) \in \mathbb{D} \mid T_{m_1}(r)^2 = \cos^2(m_2 \theta)\} \text{ where}$$

$T_{m_1}(r) = \cos(m_1 \arccos r)$  is the classical univariate Chebyshev polynomial of the first kind of degree  $m_1$ .<sup>1</sup> The nodes derived from the sampling grid correspond exactly to the points where these algebraic functions reach their extrema ( $T_{m_1}(r)^2 = 1$ ) or roots ( $T_{m_1}(r)^2 = 0$ ).<sup>1</sup>

This translates the node set into the union of two disjoint, finite interlacing grids  $I_0^{(m)}$  and  $I_1^{(m)}$  in polar coordinates, where  $r_{i_1}^{(m_1)} = \cos(\frac{i_1}{2m_1}\pi)$  and  $\theta_{i_2}^{(m_2)} = \frac{i_2}{2m_2}\pi$ .<sup>1</sup> The elegance of this formulation is that it constructs a discrete function space  $\mathcal{L}(I^{(m)})$  equipped with an inner product space and discrete integration weights  $w_i^{(m)}$ . A spectral index set  $\Gamma^{(m)}$  can then be used to select basis functions  $\chi_\gamma^{(m)}$  that are mutually orthogonal.<sup>1</sup>

When mapping this to a continuous interpolation space  $\Pi^{(m)}$  using a parity-modified Chebyshev-Fourier basis  $X_\gamma(r, \theta) = T_{\gamma_1}(r)e^{i\gamma_2\theta}$ , the interpolation problem is proven to be unisolvant.<sup>1</sup> The interpolant perfectly reconstructs the given data, and via algorithms equivalent to the 2D-FFT, it can be calculated efficiently. Furthermore, for a rectangular spectral index set  $\Gamma_\square^{(m)}$ , the Lebesgue constant  $\Lambda_\square^{(m)}$  (which measures the numerical condition of the interpolation scheme) is strictly bounded by  $C_\square \ln(m_1 + 1) \ln(m_2 + 1)$ .<sup>1</sup> This logarithmic bound guarantees that the scheme converges rapidly for smooth functions and remains highly stable as the density of the self-intersection points increases.<sup>1</sup>

## Phase Collision Mapping: From Continuous Trajectories to Discrete Nodes



Erb's methodology relies on identifying phase collisions in the parametric domain and decoupling the frequency components using Bezout's identity. This reduces the infinite continuous domain into a finite, discrete grid of interpolation nodes.

The dual representation utilizing parametric phase collisions decoupled via Bézout's identity and implicit boundaries defined by Chebyshev varieties forms the baseline blueprint. The remainder of this report traces the deployment of this blueprint across varying complex

geometric parameterizations.

## Bivariate and Spherical Lissajous Curves

The most immediate geometric relatives to the rhodonea curves are Lissajous curves. Erb and his collaborators have extensively studied polynomial interpolation on the node points of Lissajous curves in both bivariate (planar) and spherical contexts, driven largely by their utility in Magnetic Particle Imaging (MPI) and general numerical approximation.<sup>4</sup> The transition from rhodonea to Lissajous is mathematically seamless because both systems are fundamentally defined by the superposition of distinct harmonic motions bounded by a frequency vector.

### Bivariate Lissajous Nodes

In the planar case, a Lissajous curve is strictly parametrically defined as:

$\ell_\alpha^{(m)}(t) = \left( \cos(m_2 t), \cos\left(m_1 t - \frac{\alpha}{m_2} \pi\right) \right)$  where  $\alpha \in \mathbb{R}$  acts as the phase shift parameter.<sup>4</sup> Unlike the polar rhodonea curve bounded by the unit disk, this Lissajous curve is naturally bounded by the square domain  $[-1, 1]^2$ .

Erb categorizes planar Lissajous curves into two distinct classes based on their phase shift: degenerate curves and non-degenerate curves.<sup>4</sup>

1. **Degenerate Curves ( $\alpha \in \mathbb{Z}$ )**: These curves possess a property where the trajectory is traversed twice during a full  $2\pi$  period—once forward and once backward. Through the phase-matching logic (similar to the rhodonea evaluation), the self-intersection points correspond to times where the curve is essentially traversed four times.<sup>4</sup> Calculating the nodes using the sampling points  $t_{l,0}^{(m)} = \frac{l\pi}{m_1 m_2}$  yields exactly  $\frac{(m_1-1)(m_2-1)}{2}$  self-intersection points.<sup>4</sup> Furthermore, when the specific frequency parameters  $(m_1, m_2)$  are chosen as sequential integers  $(k, k+1)$  or  $(k+1, k)$ , the resulting self-intersection points form the Padua points—a renowned, mathematically optimal node set for bivariate polynomial interpolation.<sup>4</sup>
2. **Non-Degenerate Curves ( $\alpha \notin \mathbb{Z}$ )**: These curves maintain a strict time period of  $2\pi$  without retracing their own path in reverse.<sup>4</sup> Consequently, the lack of exact trajectory overlap expands the volume of discrete self-intersections to  $2m_1 m_2 - m_1 - m_2$  points.<sup>4</sup> The nodes are identified through the union of two sampling sets  $\text{LS}_{\alpha,0}^{(m)}$  and  $\text{LS}_{\alpha,1}^{(m)}$  evaluated at  $t_{l,0}^{(m)}$  and  $t_{l,\alpha}^{(m)}$  respectively.<sup>4</sup>

Because planar Lissajous curves are intrinsically linked to Chebyshev polynomials (indeed, they represent Chebyshev varieties with genus zero), the interpolation space operates using a standard d-variate polynomial basis rather than the polar Chebyshev-Fourier hybrid.<sup>11</sup>

However, the core unisolvence and the  $\mathcal{O}(N \log N)$  FFT-based extraction of coefficients remains completely intact.

## Spherical Lissajous Nodes

Projecting this kinematic concept onto a 3D manifold introduces complex topological characteristics. A spherical Lissajous curve on the unit sphere  $\mathbb{S}^2$  is parametrically defined as:

$$\ell_\alpha^{(m)}(t) = (\sin(m_2 t) \cos(m_1 t - \alpha\pi), \sin(m_2 t) \sin(m_1 t - \alpha\pi), \cos(m_2 t))$$

where  $t \in \mathbb{R}$ .<sup>9</sup> This parameterization models the superposition of a latitudinal and a longitudinal harmonic oscillation.<sup>9</sup>

To locate the self-intersection points on the sphere, the phase collision methodology utilizes two interlacing sets of sampling points for  $l \in \{0, 1, \dots, 2m_1 m_2 - 1\}$ :  $t_l^{(m)} = \frac{l\pi}{m_1 m_2}$ , and  $t_{l+1/2}^{(m)} = \frac{(l+1/2)\pi}{m_1 m_2}$ .<sup>9</sup>

The geometric topology of the self-intersections is strictly governed by the parity of the longitudinal frequency  $m_2$ .

- If  $m_2$  is even: The curve traverses the north and south poles exactly  $m_2$  times per  $2\pi$  period.<sup>9</sup> The poles act as highly degenerate singularities. The algorithm yields  $m_2(m_1 - 1) + 2$  total intersection points, consisting of the 2 poles and  $m_2(m_1 - 1)$  non-polar double points.<sup>9</sup>
- If  $m_2$  is odd: The curve also traverses the poles  $m_2$  times, but the non-polar double points shift to the half-step sampling grid  $t_{l+1/2}^{(m)}$ , yielding a total of  $m_1 m_2 + 2$  intersection points.<sup>9</sup>

As established in Erb's framework, these spherical nodes form the union of two interlacing rectangular grids across the spherical coordinates  $(\theta, \varphi)$ . The latitudinal angles are

quantized as  $\theta_{i_1}^{(m_1)} = \frac{i_1}{m_1}\pi \in [0, \pi]$ , and the longitudinal angles as

$\varphi_{i_2}^{(m_2)} = \frac{i_2}{m_2}\pi \in [0, 2\pi]$ .<sup>9</sup> This grid supports a discrete orthogonality structure for

spherical harmonics, enabling stable, logarithmically bounded spectral interpolation over the surface of the sphere.<sup>9</sup> The successful deployment of time-equidistant sampling and Bézout decoupling across both the flat square  $[-1, 1]^2$  and the curved  $\mathbb{S}^2$  confirms that the technique is theoretically universal for geometries dictated by bounded, rationally related harmonic frequencies.

## Epitrochoids and Hypotrochoids: Kinematic Varieties

Moving beyond standard harmonic superposition, epitrochoids and hypotrochoids introduce kinematic complexity. These roulette curves are geometrically defined by tracing a point  $P$  rigidly attached to a moving circle of radius  $r$  rolling without slipping along a fixed circle of radius  $R$ . The point  $P$  is located at a distance  $d$  from the center of the rolling circle.<sup>15</sup>

Depending on the configuration, these curves map to several distinct historical geometries:

- **Epitrochoids** (rolling on the outside): Include the epicycloid (when  $d = r$ ), the limacon of Pascal (when  $R = r$ ), and the nephroid (when  $R = 2r, d = r$ ).<sup>15</sup>
- **Hypotrochoids** (rolling on the inside): Include the hypocycloid (when  $d = r$ ), the astroid (when  $R = 4r, d = r$ ), and the deltoid (when  $R = 3r, d = r$ ).<sup>15</sup>

## Parametric Phase Decoupling in the Complex Plane

In the complex plane, the parametric equations for an epitrochoid can be elegantly expressed as a combination of complex exponentials:  $w = f(t) = (R + r)e^{it\lambda_1} - de^{it\lambda_2}$  where  $\lambda_1 = 1$  and  $\lambda_2 = \frac{R+r}{r}$ .<sup>16</sup> For a hypotrochoid, the rolling circle is internal, altering the radius addition to subtraction  $R - r$  and inverting the rotation direction.<sup>15</sup>

The defining feature of these curves—and the key to unlocking Erb's algorithms—is the ratio of the radii. When the ratio  $(R + r)/r$  (or  $(R - r)/r$ ) is a rational number, it can be expressed as  $p/q$ , where  $p$  and  $q$  are positive, coprime integers ( $p > q$ ).<sup>16</sup> Under this rational constraint, the curve is strictly closed and periodic. The period of a hypotrochoid, for example, is the least integer  $\rho$  such that  $\rho \times 2\pi r$  is a multiple of  $2\pi R$ , effectively equal to  $r/\gcd(r, R)$ .<sup>15</sup>

To find the self-intersection points using Erb's phase collision technique, one must locate two distinct times  $t_1$  and  $t_2$  where  $f(t_1) = f(t_2)$ . By normalizing the time parameter to

$s = t/q$ , the frequencies rescale directly to the integers  $q$  and  $p$ .<sup>16</sup> The self-intersection condition then becomes a search for points where:  $e^{iqs_1} - \gamma e^{ips_1} = e^{iqs_2} - \gamma e^{ips_2}$  where the geometric coefficient  $\gamma = \frac{d}{R+r}$  (or  $\frac{d}{R-r}$  for hypotrochoids) governs the depth of the intersection loops.<sup>16</sup>

Because  $p$  and  $q$  are integers, this system is a finite trigonometric polynomial. This allows for the precise deployment of Bézout's identity to decouple the arguments. Just as with the rhodonea curves, the temporal collisions occur exactly on a time-equidistant grid

$t_l \propto l\pi/(pq)$ . The precise locations of the intersections are inherently defined by the integer variables  $p$  and  $q$ , forming a sequence of interlocking nodes within the epicyclic or hypocyclic annulus.

## Algebraic Geometry and Chebyshev Varieties

The connection to Erb's framework runs deeper when viewed through the lens of algebraic geometry. The Cartesian coordinates of both epitrochoids and hypotrochoids can be implicitly defined through the elimination of the parameter  $t$ . Because their parameterizations rely on integer multiples of angles ( $ps$  and  $qs$ ), their coordinates can be expressed entirely using Chebyshev polynomials of the first kind,  $T_q$  and  $T_p$ .<sup>19</sup>

Consequently, epitrochoids and hypotrochoids belong to a specialized family of plane affine algebraic curves known as Chebyshev varieties.<sup>13</sup> These varieties are known to have a genus of zero, but they can possess an arbitrarily high degree.<sup>13</sup> The algebraic mapping is crucial because it allows the application of Bézout's theorem.

While Bézout's *lemma* ( $ax + by = 1$ ) is a tool from number theory used by Erb to decouple the parametric phase frequencies<sup>1</sup>, Bézout's *theorem* is a fundamental principle of algebraic geometry.<sup>22</sup> Bézout's theorem states that the number of common intersection points of two algebraic curves of degree  $d_1$  and  $d_2$  is at most  $d_1 \times d_2$ .<sup>22</sup> When the single parametric equation of a trochoid is converted into its implicit algebraic form, the maximum degree is heavily dependent on  $p$  and  $q$ . For example, the maximum algebraic degree of an

epitrochoid is bounded by  $p + q$ , and a hypotrochoid by  $p - q$ .<sup>23</sup>

This guarantees that the number of self-intersections is strictly finite and deterministic. Because the roots of the differences of Chebyshev polynomials lie on highly regular, predictable grids (the Chebyshev nodes), the self-intersection points of any rational epitrochoid or hypotrochoid can be isolated by sampling the curve at equidistant intervals.<sup>19</sup> Thus, Erb's sampling technique can extract these intersections perfectly, allowing the "spider-like" loops of high-order trochoids to serve as stable interpolation nodes.<sup>23</sup>

Curve Type	Frequency Parameters	Periodicity Condition	Maximum Algebraic Degree (Bezout Bound)	Interpolation Space Geometry
Rhodonea (Rose)	$(m_1, m_2)$	$2\pi$ or $\pi$	$2m_1 +$	Unit Disk
Bivariate Lissajous	$(m_1, m_2,$ phase $\alpha$	$2\pi$	$\max(m_1, m_2)$	Square $[-1, 1]^2$
Spherical Lissajous	$(m_1, m_2,$ phase $\alpha$	$2\pi$	$\max(m_1, m_2)$	Unit Sphere $\mathbb{S}^2$
Epitrochoid	$R, r \rightarrow$	$2q\pi$	$p +$	Epicyclic Annulus
Hypotrochoid	$R, r \rightarrow$	$2q\pi$	$p -$	Hypocyclic Annulus

## The Generalized Gielis Superformula

Applying spectral node finding to the generalized Gielis superformula represents a significant leap in mathematical complexity due to the severe non-linearity of the equation. Originally proposed by Johan Gielis in 2003 as a unified framework to describe a vast array of natural and abstract shapes—ranging from square bamboos and diatoms to starfish and spiral shells—the superformula extends Gabriel Lamé's curves (superellipses) into polar

coordinates.<sup>6</sup>

$$\text{The Gielis superformula is defined as: } \rho(\theta) = \left( \left| \frac{1}{a} \cos \left( \frac{m\theta}{4} \right) \right|^{n_2} + \left| \frac{1}{b} \sin \left( \frac{m\theta}{4} \right) \right|^{n_3} \right)^{-\frac{1}{n_1}}$$

where  $a, b \in \mathbb{R}^+$  act as scaling factors,  $m \in \mathbb{R}^+$  defines the rotational symmetry, and  $n_1, n_2, n_3 \in \mathbb{R}^+$  dictate the curvature and shape of the resulting boundary.<sup>30</sup>

## Rational Symmetries and Self-Intersection

When the symmetry parameter  $m$  is an integer, the formula generates a simple, closed, non-intersecting boundary repeating every  $2\pi$ .<sup>30</sup> However, when  $m$  is a rational number—expressed as  $m = p/q$  where  $p$  and  $q$  are relatively prime positive integers—the function generates what is termed a Rational Gielis Curve (RGC).<sup>30</sup>

To close an RGC, the angular parameter  $\theta$  must traverse the interval  $[0, 2q\pi]$ .<sup>30</sup> This means the curve wraps around the origin  $q$  times before reconnecting. In doing so, it generates complex polygrams (e.g., a pentagram-like figure when  $m = 5/2$ ) that exhibit extensive and predictable self-intersections.<sup>33</sup> These self-intersecting lines act as "curved knives," dividing the internal space into distinct topological sectors or zones.<sup>35</sup>

Finding these self-intersection points analytically is challenging. In the rhodonea framework, intersections occurred primarily where the radial distance  $\rho(\theta)$  was exactly 0 (the origin) or at the outer boundary extrema.<sup>1</sup> For a Gielis curve, the absolute value operators and fractional exponents prevent standard trigonometric sum-to-product expansions or direct conversion into a single polynomial implicit equation.<sup>37</sup>

A self-intersection at a non-origin coordinate occurs where two distinct angles  $\theta_1, \theta_2 \in$

Because the radius function  $\rho(\theta)$  has an inherent internal periodicity of  $4\pi/m = 4q\pi/p$ , the condition  $\rho(\theta) = \rho(\theta + 2k\pi)$  transforms into a Diophantine alignment problem directly analogous to Erb's phase collisions. The radial equality holds if and only if the angular offset  $2k\pi$  is an exact integer multiple of the radial period  $4q\pi/p$ . This requires the fraction  $\frac{k\cdot p}{2q}$  to be an integer. By calculating the values of  $k \in \{1, \dots, q - 1\}$  that satisfy this ratio,

one can isolate the specific angular domains where the RGC crosses itself.

## R-Functions and Implicit Potential Fields

To utilize the self-intersections of Rational Gielis Curves as valid mathematical nodes for boundary value problems, the parametric formulation must be converted into an implicit algebraic field. This is achieved using the theory of R-functions (Rvachev functions).<sup>32</sup> R-functions form a natural alliance with superellipses, allowing for the construction of signed potential fields with guaranteed differential properties.<sup>32</sup>

Because an RGC self-intersects, a single implicit field cannot capture the boundary without generating ambiguities at the crossing nodes.<sup>32</sup> Instead, N-ary R-conjunction and R-disjunction operations are used to perform boolean logic on the intersecting lobes of the curve.<sup>32</sup> This blends multiple potential fields into a single unified field where the zero-set corresponds exactly to the outer envelope, inner envelope, or specific internal sectors of the self-intersecting geometry.<sup>32</sup>

By overlaying Erb's equidistant angular sampling grid  $\theta_l = \frac{l\pi}{p \cdot q}$  onto these R-function-derived implicit surfaces, the exact locations of the self-intersection nodes can be computationally extracted. This mathematically transforms the overlapping petals of a Gielis polygram into a valid, discrete node set. Once extracted, these nodes allow researchers to solve complex boundary value problems—such as the Dirichlet problem for the Laplace equation—across highly irregular, starlike biological domains using semi-Fourier methods.<sup>40</sup>

# Sampling Grid Parameters for Unisolvant Interpolation Nodes

Curve Type	Frequency Variables	Normalized Domain	Node Grid Formula ( $t_l$ )	Phase Collision Bound
Rhodonea	$m = (m_1, m_2) \in \mathbb{N}^2$ <i>(relatively prime)</i>	$t \in [0, 2\pi]$ if $m_1 + m_2$ is odd $t \in [0, \pi]$ if $m_1 + m_2$ is even	$t_l^{(m)} = (l\pi) / (2m_1m_2)$ $l \in \{0, \dots, 4m_1m_2 - 1\}$	$2m_1m_2 + 1$ points in $\mathbb{D}$ (Center traversed $2m_2$ or $m_2$ times)
Bivariate Lissajous	$m = (m_1, m_2)$ , phase shift $\alpha$ <i>(relatively prime)</i>	$t \in [0, 2\pi]$	$t^{(m)}_{l,\alpha} = ((l+\alpha)\pi) / (m_1m_2)$ $l \in \{0, \dots, 2m_1m_2 - 1\}$	$2m_1m_2 - m_1 - m_2$ (Non-degenerate curves)
Epitrochoid	$(R + r) / r = p/q$ <i>(<math>p, q</math> positive, coprime integers)</i>	$t = qs$	$w = (R+r)e^{it} - de^{it(R+r)/r}$ <i>Discrete extraction defined parametrically</i>	Described by Theorem 5.6 and Corollary 5.8
Rational Gielis	$m = p/q$ <i>(<math>p</math> sectors, <math>q</math> intersections)</i>	$t \in [0, 2q\pi]$	Repeated continuous domain. <i>Cycle derived from <math>2q\pi</math> intervals.</i>	Bounded by $q$ (Max self-intersections)

To locate self-intersection points across varying geometries, the time domain must be sampled using specific equidistant intervals derived from the curve's rational frequency components.

Data sources: Erb (2018) - Rhodonea curves, [Wolfgang Erb \(Lissajous\)](#), [Epitrochoid \(arXiv:2304.09940\)](#), [Gielis Superformula \(MDPI\)](#)

## The Farris "Mystery" Curve: Finite Fourier Series

The Farris "mystery" curve, extensively detailed by Frank A. Farris in his exploration of symmetry and wallpaper patterns, represents an ideal candidate for the direct application of Erb's spectral node algorithms.<sup>7</sup> Unlike kinematically derived trochoids or the absolute-value-bounded superformula, the Farris curve is explicitly defined as a finite

complex Fourier series.

The classic iteration of the Farris curve, which exhibits a striking five-fold symmetry, is defined in the complex plane by the equation:  $f(t) = e^{it} + \frac{1}{2}e^{6it} + \frac{i}{3}e^{-14it}$  where  $t$  ranges from  $0$  to  $2\pi$ .<sup>7</sup>

Expressed parametrically in standard Cartesian coordinates, this separates into:

$$x(t) = \cos(t) + \frac{1}{2}\cos(6t) + \frac{1}{3}\sin(14t) \quad y(t) = \sin(t) + \frac{1}{2}\sin(6t) + \frac{1}{3}\cos(14t)$$

.<sup>7</sup>

The geometric "mystery" of its five-fold rotational symmetry emerges directly from the mathematical relationships of its frequency multipliers relative to the fundamental frequency ( $1t$ ). The differences are  $6 - 1 = 5$  and  $-14 - 1 = -15$ . Because both differences are integer multiples of  $5$ , the resulting spatial projection is perfectly symmetric under rotations of  $2\pi/5$ .<sup>44</sup>

Because the Farris curve is strictly composed of a finite sum of trigonometric terms, finding its self-intersection points is mathematically isomorphic to finding the roots of a bounded spectral system. A self-intersection point requires that the spatial position at two different times is identical:  $f(a) = f(b)$  where  $a \neq b \pmod{2\pi}$ .<sup>7</sup>

Expanding the real component of this equation yields:

$$\cos(a) - \cos(b) + \frac{1}{2}(\cos(6a) - \cos(6b)) + \frac{1}{3}(\sin(14a) - \sin(14b)) = 0$$

with a symmetric equation governing the imaginary  $y$ -components. By deploying standard sum-to-product trigonometric identities—a process highly analogous to the double-angle expansions required to find the intersections of a standard 4-petal curve like  $r = \sin(2t)$ —the terms containing the difference  $\frac{a-b}{2}$  can be factored out of the system.<sup>46</sup>

This algebraic factorization isolates the specific roots responsible for the self-intersections.

Because the highest frequency present in the system is  $14t$ , the maximum algebraic degree of the equivalent implicit system is strictly capped. Once again, Bézout's theorem ensures that the maximum number of self-intersections is both finite and deterministic.<sup>22</sup>

Applying Erb's rhodonea-based node algorithms to the Farris curve is highly efficient. The specific integer frequencies involved ( $1, 6, 14$ ) dictate that an equidistant sampling grid of

$t_l = \frac{l\pi}{N}$  (where  $N$  is derived from the least common multiple of the frequency combinations, suitably padded to avoid aliasing) will sample the curve's self-intersections exactly. If a mathematician uses these self-intersection points as nodes, they can define a spectral interpolation space spanned by the corresponding Fourier basis functions.<sup>1</sup>

Furthermore, because the Farris curve does not rely on fractional exponents or non-differentiable absolute value operators, the computation of the spectral expansion

coefficients  $c_\gamma(f)$  can be performed natively using the discrete fast Fourier transform (FFT) on the finite abelian group  $(\mathbb{Z}/N\mathbb{Z})$ . This perfectly mirrors the computational efficiency of Erb's Algorithm 1 developed for the unit disk.<sup>1</sup>

## Algorithmic Implementation, Quadrature, and Convergence

The mathematical viability of adapting Erb's node-finding algorithms is only half the equation; one must also evaluate the numerical stability and convergence properties of the resulting interpolants. If researchers are to replace standard tensor-product grids with the discrete self-intersection nodes of these complex planar curves, the scheme must resist polynomial oscillation and exhibit robust error bounds.<sup>1</sup>

### The Lebesgue Constant and Spectral Stability

The numerical condition of any interpolation problem is measured by its Lebesgue constant,  $\Lambda^{(m)}$ , which serves as an upper bound on how small errors in the sampled function amplify the error of the interpolant in the uniform norm.<sup>1</sup> Erb proved that for rhodonea curves

employing a rectangular spectral index set  $\Gamma_{\square}^{(m)}$ , the Lebesgue constant grows only logarithmically relative to the frequency parameters:

$$\Lambda_{\square}^{(m)} \leq C_{\square} \ln(m_1 + 1) \ln(m_2 + 1) \text{ where } C_{\square} \text{ is a constant independent of } m.$$

This favorable, slow logarithmic growth is not an exclusive, isolated property of rhodonea curves. Rather, it is a fundamental consequence of evaluating a discrete orthogonality structure across interlaced grids derived from rational frequency combinations.<sup>1</sup>

Consequently, this stability transfers directly to the other curve families discussed:

1. **For Trochoids (Epitrochoids/Hypotrochoids):** Because their kinematics map exactly to Chebyshev varieties, polynomial interpolation evaluated on their self-intersection nodes will similarly experience logarithmic growth in the Lebesgue constant.<sup>20</sup> If the function being interpolated is analytically smooth, a multivariate Jackson inequality for trigonometric functions guarantees that the uniform convergence of the interpolant

towards the true function accelerates faster than any polynomial rate as the frequencies  $p$  and  $q$  increase.<sup>1</sup>

2. **For Farris Curves:** Because the nodes represent the exact roots of finite Fourier series, polynomial interpolation on these self-intersections operates as trigonometric interpolation over non-uniform but rationally spaced points. Provided the basis functions are chosen to encompass the bounded frequency support of the Farris equation (up to  $14t$ ), the numerical stability is inherently maintained.<sup>7</sup>
3. **For Gielis Curves:** The numerical condition is slightly more volatile. The sharp corners and high curvature generated by extreme parameter values (e.g.,  $n_1 \gg 1$ ) can introduce steep gradients that trigger Runge's phenomenon if standard polynomials are applied naively.<sup>19</sup> However, stability can be restored by warping the interpolation space. If the parity-modified Chebyshev-Fourier basis is mathematically scaled by the  $\rho(\theta)$  function itself—similar to how Erb's basis naturally incorporates the boundaries of the unit disk—the logarithmic stability bounds can be preserved.<sup>1</sup>

## Computational Extraction and Quadrature

From a software and implementation perspective, utilizing these curves as sampling trajectories requires mapping the calculated nodes into a multi-dimensional array

representing the index sets  $I_0$  and  $I_1$ .<sup>1</sup> Once the data is collected at the precise self-intersection points of a hypotrochoid or a rational Gielis curve, the algorithm developed by Erb dictates that the function  $g(i)$  must be extended symmetrically across the dual group  $J^{(m)}$  utilizing block-mirror centrosymmetric (BMC) structures.<sup>1</sup>

This symmetry extension is crucial. It allows the continuous spectral coefficients  $c_\gamma(f)$  to be computed rapidly via a double Fourier transform over the finite abelian group  $(\mathbb{Z}/4m_1\mathbb{Z}) \times (\mathbb{Z}/4m_2\mathbb{Z})$ .

Furthermore, once the coefficients are isolated, they empower the execution of a Clenshaw-Curtis quadrature rule. By explicitly integrating the basis functions  $X_\gamma \in \Pi^{(m)}$  over the respective domain, the complex integral of any sampled function over the irregular boundary of a trochoid or a Farris star can be reduced to a discrete sum:

$$Q(f) = \sum_{k=0}^{\lfloor m_1/2 \rfloor} \frac{c_{(4k,0)}(f)}{1-4k^2}.$$
<sup>1</sup> This proves that spectral integration and function reconstruction can be reliably performed over highly complex, non-Cartesian boundaries using self-intersecting trajectories as the sole source of geometric data.<sup>1</sup>

# Conclusion

The spectral interpolation framework established by Wolfgang Erb for rhodonea curves relies on two fundamental mathematical pillars: the parameterization of the domain boundaries by rationally related harmonic frequencies, and the subsequent resolution of continuous phase collisions via Bézout's identity to form a stable, discrete node grid. The analysis synthesized in this report demonstrates that this exact methodology is highly extensible and robust across varied geometries.

For Lissajous curves and the Farris "mystery" curve, the algorithmic extension is nearly isomorphic, as both rely entirely on the exact resolution of finite trigonometric polynomials and Fourier series. For epitrochoids and hypotrochoids, the algebraic mapping to Chebyshev varieties guarantees that their complex, gear-like self-intersection nodes can be systematically located, yielding logarithmically bounded polynomial interpolation. Finally, while the generalized Gielis superformula introduces significant non-linear complexity through absolute value operators, the underlying rational periodicity of its angular parameters allows for the precise isolation of self-intersection domains. By coupling Erb's discrete angular sampling matrices with R-function boolean logic, researchers can achieve unisolvent spectral interpolation over virtually any self-intersecting natural or abstract shape. This synthesis effectively broadens the scope of spectral approximation theory, linking continuous kinematic geometries with highly optimized discrete sampling arrays.

## Works cited

1. Erb - 2018 - Rhodonea curves as sampling trajectories for spect.pdf
2. Scan patterns of rotational Risley prisms: study with regard to... - ResearchGate, accessed February 15, 2026,  
[https://www.researchgate.net/figure/Scan-patterns-of-rotational-Risley-prisms-study-with-regard-to-negative-values-of-M\\_fig7\\_323268179](https://www.researchgate.net/figure/Scan-patterns-of-rotational-Risley-prisms-study-with-regard-to-negative-values-of-M_fig7_323268179)
3. COMPENDIUM USAMO - Toomates, accessed February 15, 2026,  
<http://www.toomates.net/biblioteca/CompendiumUSAMO.pdf>
4. Wolfgang Erb | Lissajous Curves, accessed February 15, 2026,  
<https://www.math.unipd.it/~erb/Lissajous.html>
5. Epitrochoids and Hypotrochoids Together Again - Professor Dresden's Home Page, accessed February 15, 2026,  
<https://dresden.academic.wlu.edu/files/2024/07/TrochoidsThirdSubmission.pdf>
6. A Point-Theory of Morphogenesis - Preprints.org, accessed February 15, 2026,  
[https://www.preprints.org/frontend/manuscript/4bdf923bd42353d02d2da6da361888e/download\\_pub](https://www.preprints.org/frontend/manuscript/4bdf923bd42353d02d2da6da361888e/download_pub)
7. Solution: 'Creating Art With Mathematics' | Quanta Magazine, accessed February 15, 2026,  
<https://www.quantamagazine.org/solution-creating-art-with-mathematics-2015030/>
8. Wolfgang Erb | Rhodonea curves, accessed February 15, 2026,

- <https://www.math.unipd.it/~erb/rhodonea.html>
- 9. Wolfgang Erb | Spherical Lissajous Curves, accessed February 15, 2026,  
<https://www.math.unipd.it/~erb/LSphere.html>
  - 10. Chebyshev varieties | Request PDF - ResearchGate, accessed February 15, 2026,  
[https://www.researchgate.net/publication/393997529\\_Chebyshev\\_varieties](https://www.researchgate.net/publication/393997529_Chebyshev_varieties)
  - 11. Multivariate polynomial interpolation on Lissajous-Chebyshev nodes  
arXiv:1511.04564v2 [math.NA] 21 Aug 2017, accessed February 15, 2026,  
<https://arxiv.org/pdf/1511.04564>
  - 12. Mathematics Mind Map | PDF | Algebraic Geometry - Scribd, accessed February 15, 2026, <https://www.scribd.com/document/520363930/Mathematics-Mind-Map>
  - 13. Examples of plane algebraic curves - MathOverflow, accessed February 15, 2026,  
<https://mathoverflow.net/questions/352957/examples-of-plane-algebraic-curves>
  - 14. A spectral interpolation scheme on the unit sphere based on the nodes of spherical Lissajous curves - arXiv, accessed February 15, 2026,  
<https://arxiv.org/pdf/1802.06546>
  - 15. NOTES ON HYPOTROCHOIDS AND EPITROCHOIDS - WebCMS3, accessed February 15, 2026,  
<https://webcms3.cse.unsw.edu.au/files/77a3632422040bb6f33386b1818982b7b9fc8fbe6de5f4f62eda4af9ee1fafd3>
  - 16. Periodic functions: self-intersections, local singular points ... - arXiv, accessed February 15, 2026, <https://arxiv.org/pdf/2304.09940>
  - 17. Epitrochoids, Hypotrochoids, Peritrochoids - Walter Fendt, accessed February 15, 2026, [https://www.walter-fendt.de/html5/men/epihypotrochoids\\_en.htm](https://www.walter-fendt.de/html5/men/epihypotrochoids_en.htm)
  - 18. Marks' - Standard Handbook for Mechanical Engineers - Bulk Material Handling Equipment, accessed February 15, 2026,  
<https://iem.ca/pdf/resources/Marks-standard-handbook-for-mechanical-engineers.pdf>
  - 19. Chebyshev polynomials - Wikipedia, accessed February 15, 2026,  
[https://en.wikipedia.org/wiki/Chebyshev\\_polynomials](https://en.wikipedia.org/wiki/Chebyshev_polynomials)
  - 20. [Literature Review] Chebyshev Varieties - Moonlight, accessed February 15, 2026,  
<https://www.themoonlight.io/en/review/chebyshev-varieties>
  - 21. [2401.12140] Chebyshev Varieties - arXiv, accessed February 15, 2026,  
<https://arxiv.org/abs/2401.12140>
  - 22. Bézout's theorem - Wikipedia, accessed February 15, 2026,  
[https://en.wikipedia.org/wiki/B%C3%A9zout%27s\\_theorem](https://en.wikipedia.org/wiki/B%C3%A9zout%27s_theorem)
  - 23. Plane Algebraic Curves [PDF] [410jbaim51h0] - VDOC.PUB, accessed February 15, 2026, <https://vdoc.pub/documents/plane-algebraic-curves-410jbaim51h0>
  - 24. Rose - MATHCURVE.COM, accessed February 15, 2026,  
<https://mathcurve.com/courbes2d.gb/rosace/rosace.shtml>
  - 25. Approximation Theory – Lecture 7 7 Chebyshev polynomials - DAMTP, accessed February 15, 2026, <https://www.damtp.cam.ac.uk/user/na/PartIIIlat/b07.pdf>
  - 26. Closed-form solution of repeat ground track orbit design and constellation deployment strategy - ResearchGate, accessed February 15, 2026,  
[https://www.researchgate.net/publication/348039781\\_Closed-form\\_solution\\_of\\_repeat\\_ground\\_track\\_orbit\\_design\\_and\\_constellation\\_deployment\\_strategy](https://www.researchgate.net/publication/348039781_Closed-form_solution_of_repeat_ground_track_orbit_design_and_constellation_deployment_strategy)

27. Superellipses to Superformula: The impact of Gielis Transformations - Research Outreach, accessed February 15, 2026,  
<https://researchoutreach.org/articles/superellipses-superformula-impact-gielis-transformations/>
28. The Harmonic Pattern Function: A Mathematical Model Integrating Synthesis of Sound and Graphical Patterns | UCSB MAT, accessed February 15, 2026,  
[https://www.mat.ucsb.edu/Dissertations/The\\_Harmonic\\_Pattern\\_Function\\_Lance\\_Putnam.pdf](https://www.mat.ucsb.edu/Dissertations/The_Harmonic_Pattern_Function_Lance_Putnam.pdf)
29. A robust evolutionary algorithm for the recovery of rational Gielis curves - ResearchGate, accessed February 15, 2026,  
[https://www.researchgate.net/publication/237047990\\_A\\_robust\\_evolutionary\\_algorithm\\_for\\_the\\_recovery\\_of\\_rational\\_Gielis\\_curves](https://www.researchgate.net/publication/237047990_A_robust_evolutionary_algorithm_for_the_recovery_of_rational_Gielis_curves)
30. A New Objective Function for the Recovery of Gielis Curves - MDPI, accessed February 15, 2026, <https://www.mdpi.com/2073-8994/12/6/1016>
31. The Generalized Gielis Geometric Equation and Its Application - MDPI, accessed February 15, 2026, <https://www.mdpi.com/2073-8994/12/4/645>
32. A New Potential Function for Self Intersecting Gielis Curves with Rational Symmetries., accessed February 15, 2026,  
[https://www.researchgate.net/publication/220869086\\_A\\_New\\_Potential\\_Function\\_for\\_Self\\_Intersecting\\_Gielis\\_Curves\\_with\\_Rational\\_Symmetries](https://www.researchgate.net/publication/220869086_A_New_Potential_Function_for_Self_Intersecting_Gielis_Curves_with_Rational_Symmetries)
33. The general case of cutting of Generalized Möbius-Listing surfaces and bodies | 4open, accessed February 15, 2026,  
[https://www.4open-sciences.org/articles/fopen/full\\_html/2020/01/fopen200013/fopen200013.html](https://www.4open-sciences.org/articles/fopen/full_html/2020/01/fopen200013/fopen200013.html)
34. Universal Equations – A Fresh Perspective – Athena Publishing, accessed February 15, 2026, <https://www.athena-publishing.com/journals/gandf/articles/66/view>
35. The general case of cutting of Generalized Mbius-Listing surfaces and bodies - 4open, accessed February 15, 2026,  
<https://www.4open-sciences.org/articles/fopen/pdf/2020/01/fopen200013.pdf>
36. GENERALIZED MÖBIUS-LISTING BODIES AND THE HEART - Romanian Journal of Mathematics and Computer Science, accessed February 15, 2026,  
[https://rjm-cs.utcb.ro/wp-content/uploads/2023/11/2023v13i2\\_7.pdf](https://rjm-cs.utcb.ro/wp-content/uploads/2023/11/2023v13i2_7.pdf)
37. singularities on complete algebraic varieties - Department of Mathematics | University of Miami, accessed February 15, 2026,  
<https://www.math.miami.edu/~bdeolive/sing11.pdf>
38. Integrating the Gielis Superformula. - Mathematics Stack Exchange, accessed February 15, 2026,  
<https://math.stackexchange.com/questions/1660188/integrating-the-gielis-superformula>
39. a new potential function for self intersecting gielis curves with rational symmetries - SciTePress, accessed February 15, 2026,  
<https://www.scitepress.org/Papers/2009/17982/>
40. Universal Natural Shapes: From Unifying Shape Description to Simple Methods for Shape Analysis and Boundary Value Problems | PLOS One - Research journals, accessed February 15, 2026,

<https://journals.plos.org/plosone/article?id=10.1371/journal.pone.0029324>

41. A Point-Theory of Morphogenesis - MDPI, accessed February 15, 2026,  
<https://www.mdpi.com/2227-7390/13/19/3076>
42. Creating Symmetry: The Artful Mathematics of Wallpaper Patterns by Frank A. Farris | eBook, accessed February 15, 2026,  
<https://www.barnesandnoble.com/w/creating-symmetry-frank-a-farris/1120692749>
43. COLLOQUIUM - Mathematics & Statistics Department - Sonoma State University, accessed February 15, 2026,  
<https://math.sonoma.edu/sites/math/files/colloq-sems71-80.pdf>
44. How to Create Art With Mathematics | Quanta Magazine, accessed February 15, 2026,  
<https://www.quantamagazine.org/how-to-create-art-with-mathematics-20151008/>
45. Farris Mystery Curve | Workshop.codes, accessed February 15, 2026,  
<https://workshop.codes/FAT1R>
46. How to find a self-intersection point of a parametric function? : r/math - Reddit, accessed February 15, 2026,  
[https://www.reddit.com/r/math/comments/5smqyk/how\\_to\\_find\\_a\\_selfintersection\\_point\\_of\\_a/](https://www.reddit.com/r/math/comments/5smqyk/how_to_find_a_selfintersection_point_of_a/)
47. FoCM 2017 Foundations of Computational Mathematics Barcelona, July 10th-19th, 2017, accessed February 15, 2026,  
<https://www.ub.edu/focm2017/content/FoCM2017-Book.pdf>
48. lecture 15: Chebyshev Polynomials for Optimal Interpolation, accessed February 15, 2026, <https://personal.math.vt.edu/embree/math5466/lecture15.pdf>
49. Chebyshev Polynomial Approximation to Solutions of Ordinary Differential Equations - The Aquila Digital Community, accessed February 15, 2026,  
[https://aquila.usm.edu/cgi/viewcontent.cgi?article=1000&context=undergraduate\\_theses](https://aquila.usm.edu/cgi/viewcontent.cgi?article=1000&context=undergraduate_theses)
50. Estimate self crossings of a curve parameterized by a trigonometric polynomial, accessed February 15, 2026,  
<https://mathoverflow.net/questions/199855/estimate-self-crossings-of-a-curve-parameterized-by-a-trigonometric-polynomial>
51. Gielis' superformula and regular polygons - ResearchGate, accessed February 15, 2026,  
[https://www.researchgate.net/publication/273899855\\_Gielis'\\_superformula\\_and\\_regular\\_polygons](https://www.researchgate.net/publication/273899855_Gielis'_superformula_and_regular_polygons)
52. Wolfgang Erb | Software, accessed February 15, 2026,  
<https://www.math.unipd.it/~erb/software.html>